Surface Integrity of machined additively manufactured Ti alloys

Giovanna Rotella[b], Stano Imbrogno[a], Sebastiano Candamano[b], Domenico Umbrello[a,*]

[a] *Department of Mechanical, Energy and Management Engineering, University of Calabria, Rende, CS 87036, Italy*

[b] *Department of Environmental and Chemical Engineering, University of Calabria, Rende, CS 87036, Italy*

*Corresponding author: domenico.umbrello@unical.it, Tel.: +39-0984 494820. Fax: +39-0984 494673.

Abstract

Additive manufacturing processes (AM) offer the possibility to easily fabricate three-dimensional parts with high geometrical complexity. However, the additively manufactured components often require finishing operations, such as machining, showing a different machinability than those produced with conventional processes. Thus, it is crucial to study the effect of the manufacturer suggested cutting parameters on the surface integrity of the AM components, since they can behave differently than the correspondent wrought materials. The aim of the present work is to investigate the surface and subsurface modifications induced by turning operations performed on additively manufactured titanium alloys. The material under investigation is the grade 5 titanium alloy (*Ti6Al4V*) produced by three different methods namely, Electron Beam Melting (EBM), Direct Metal Laser Sintering (DMLS) and conventionally wrought processes. The effect of such processes on machinability and surface integrity is herein extensively studied (nano-hardness, plastically deformed layers, microstructural alterations etc.). In particular, the morphological, chemical and mechanical

analyses on the pre- and post-machined samples highlight the influence of the production processes on their surface integrity underlying the need to properly redesign the machining parameters accordingly.

Keywords: *Direct Metal Laser Sintering (DMLS); Electron Beam Melting (EBM), Machining; Surface Integrity; Ti6Al4V.*

1. Introduction

Additive manufacturing techniques are successfully providing the possibility to fabricate net-shaped parts with complex geometries easier and faster than traditional manufacturing. AM are defined by the American Society for Testing and Materials (ASTM), as the "processes of joining materials to make objects from three-dimensional (3D) model data, usually layer upon layer, as opposed to subtractive manufacturing methodologies" (ASTM International F2792 - 12a, 2012). As claimed by Selcuk 2011, AM can be used to manufacture different materials from metals to polymers and they can be classified according to the energy source used to generate the products (e.g. electron beam, laser), the feeding system (powder bed versus blown powder) and the feed stock form (wire or powder). Industries are attracted from this class of manufacturing processes that offer the unique opportunity to shorten lead times, cut the costs and bypass geometrical constraints, achieving lighter and cleaner products (Thompson et al., 2015).

Various researchers have investigated the effects of certain process parameters on the microstructural characteristics, structural and mechanical properties of the additively produced parts. In particular, the components show distinct regions with different microstructure and micro-hardness leading to an inhomogeneity of the mechanical response (Shamsaei et al., 2015; Levy et al., 2003). Bordin et al. (2017) confirm that AM products often present microstructural heterogeneities and randomly dispersed defects. Moreover, the AM produced parts will drastically differ from those fabricated by

conventional processes also in terms of mechanical behavior. In fact, the thermal history of AM determines a huge change of microstructural characteristics (e.g. grain size and morphology), defect type and size, residual stresses, etc. In detail, Bordin et al. (2017) claim that AM parts often present rough and porous surfaces that need to be finished by machining, grinding and polishing processes. Martina et al. (2012) investigated the microstructural and hardness changes in plasma deposition for the additive layer manufacture of *Ti6Al4V*. They highlighted the diversity in microstructure formation (martensite and different morphology of $\alpha + \beta$ microstructure) due to the compositional gradients or thermal effects. Thus, the effects of post processing methods, such as turning, on the AM products, can be considerably different from those obtained on conventionally manufactured part that are clearly summarized from Jawahir et al. (2011). For instance, Guo et al. (2017), show that the machinability of the additively manufactured AISI 316L components is affected by the building direction (0° and 90°). In detail, they observed different magnitudes of cutting force between the samples with building orientation of 0° and 90°, consequently affecting the temperature and the tool wear. Therefore, the massive adoption of AM by industries is slowed down by the lack of knowledge on structural properties of fabricated parts, especially after post-processing treatments (machining processes). This work aims to investigate the surface and subsurface modifications induced by turning operations performed on wrought and additively manufactured titanium alloys. Particular attention is paid on examining the effects of the different AM processes (EBM and DMLS) on the surface quality and integrity when conventional cutting parameters, commonly recommended for semi-finishing operations are used. The results have been compared with those obtained by machining the wrought alloy.

2. Material and methods

The material under investigation is the grade 5 titanium alloy (*Ti6Al4V*). The machined samples were produced by three different methods namely, EBM, DMLS and wrought (drown billets obtained by

ASTM B348 thermo-mechanical treatments procedure). The EBM and DMLS are two AM processes that use powder metal as feed stock; the first one uses an electron beam as the focused source of energy, while a laser beam is employed in the second manufacturing process. The production of *Ti6Al4V* samples by EBM was carried out in vacuum (the vacuum parameters set into the chamber were $5x10^{-3}$ mbar at the beginning and $2x10^{-3}$ mbar at the end of the process) in an ARCAM EBM S12. The cylindrical samples were built up by layers of 100 µm thickness, the beam diameter was 2mm and a power of 3 kW. *Ti6Al4V* DMLS samples were produced by EOS EOSINT M270 machine. The parts were built under a protective atmosphere guaranteed by a flow of 40 l/min of *Ar*. The beam diameter was 500 µm for a melt pool diameter of 150 µm and the layer thickness of 50 µm. The power was 195 W and the scan speed was equal to 225 mm/sec. For both the AM production processes, the built up direction was along the longitudinal axis of the cylindrical samples. In EBM, before the melting phase, the powder is pre-heated and kept at a temperature above 600°C that makes the stabilization of the martensitic microstructure which is then transformed in a $\alpha + \beta$ acicular microstructure (Figure 1 a) (Yan et al., 2015; Murr, 2015; Facchini et al., 2009). In DMLS, there is no pre-heating of the powder, and the microstructure of the material produced is with martensitic α'plate containing acicular hexagonal closed-packing (hcp) phase. The post-building material is characterized by a metastable martensitic structure, which is transformed into a Widmanstätten structure (lamellae of α-phase, Figure 1 b) after a subsequent Hot Isostatic Pressing (HIP) treatment performed on the DMLS material. The HIP process is usually used to treat the AM parts helping to reduce the high residual stress induced by the AM process. Moreover, the HIP has also positive effect in porosity and internal defects reduction since it allows to melt and to compact the non-melted powder. Although HIP can surely improve the overall mechanical performance of the products since the bulk material has low defects occurrence, it unfortunately does not improve the surface roughness of the AM parts. On the other hand, special attention must be paid on the microstructure because the HIP induces the change from martensitic to lamellar microstructure leading to grain growth and lowering of mechanical properties. AM processes clearly produce parts with microstructures different

from those produced by conventional processes. For example, the EBM *Ti6Al4V* shows different prior β grains, near-equiaxed prior α grains and equiaxed-to-columnar microstructure arisen from different cooling rate (Tan et al., 2015). On the contrary, the wrought *Ti6Al4V* alloy, is characterized by equiaxed primary α grains with intergranular β grains (Figure 1 c). Before machining, the as produced materials were embedded into resin (hot mounted), grinded and gently polished. As reported in Figure 1, the samples were chemically etched with the Kroll's reagent in order to analyze the microstructure through optical microscopy. The as produced microstructure of the wrought *Ti6Al4V* is characterized by equiaxed grains with an average diameter of 4.29 μm, while the EBM and DMLS samples show an average α –lamellae thickness of 1.68 μm and 3.46 μm respectively. The *Ti6Al4V* is susceptible to the development of strong textures during thermomechanical processing, thus, X-Ray Diffraction (XRD) analyses were carried out on the as produced material to understand the texture generated by the different production methods (Figure 2). The Rigaku MiniFlex 600 X-Ray diffractometer (Rigaku Corporation, Tokyo, Japan) with CuKα radiation generated at 20 mA and 40 KV was used. All the specimens were scanned at 0.02 2θ steps integrated at a rate of 0.5s with a penetration depth of about 40μm.

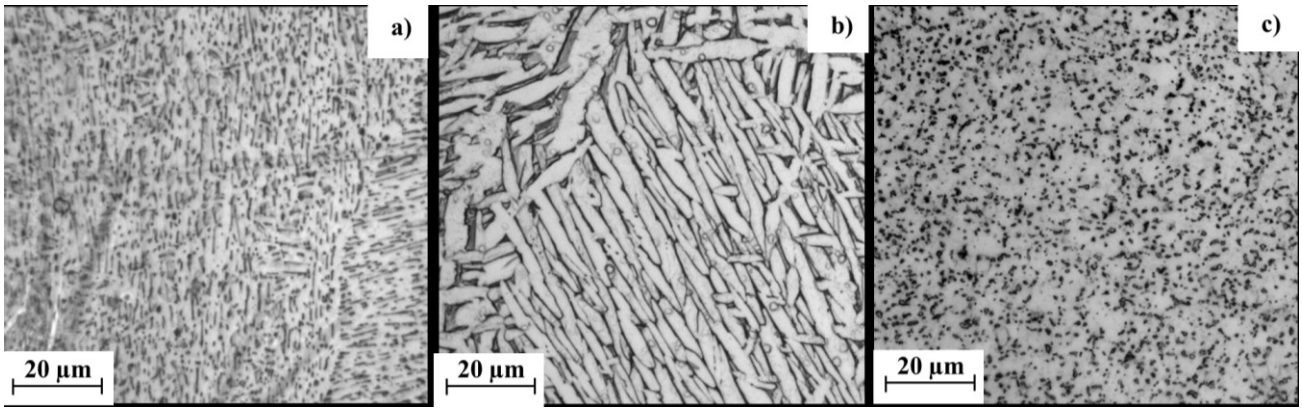

Figure 1. Optical micrographs of (a) EBM; (b) DMLS and (c) wrought *Ti6Al4V* microstructure (α phase in white, β phase in black).

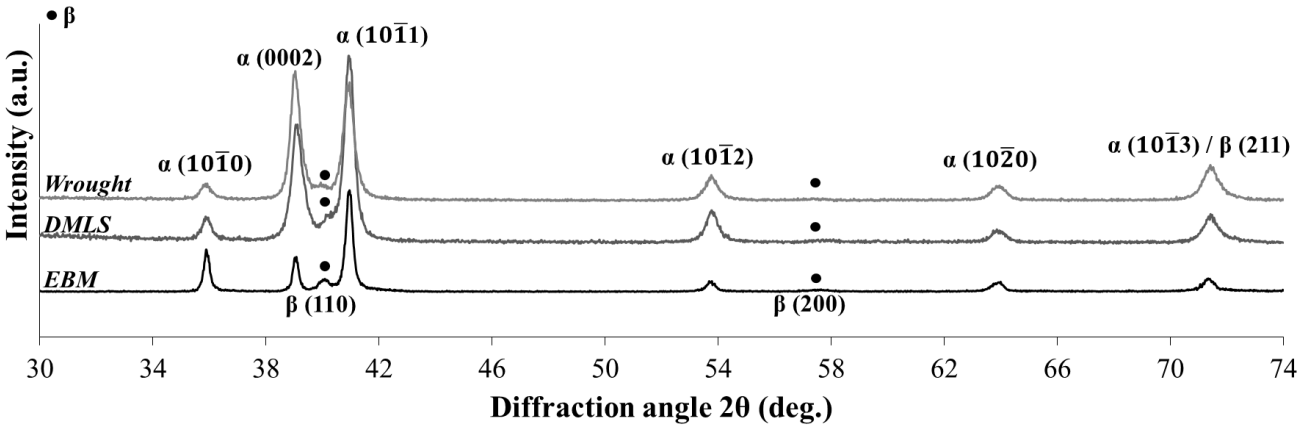

Figure 2. XRD pattern of as produced *Ti6Al4V* samples.

X-Ray Diffraction scans reveal that hcp α phase is textured on the $(1\bar{1}00)$ prism plane, (0002) basal plane and $(10\bar{1}1)$ pyramidal plane in EMB manufactured *Ti6Al4V* alloy and on (0002) basal plane and $(10\bar{1}1)$ pyramidal plane in DMLS and wrought manufactured *Ti6Al4V* alloys. Furthermore, while in EMB manufactured alloy β phase has a (100) preferred orientation and its relative peak is clearly distinguished, in DMLS and wrought alloys it is partially overlapped by $(10\bar{1}1)$ *Ti-α* peak, that consequently, results dissymmetric. All the samples show a weak peak at ≈58° 2θ corresponding to (200) reflection of β phase.

Moreover, indentation measurements were carried out using a nano-indentation platform provided with a Berkovic tip. The measurement parameters were set equal to 20 mN of load and 10 s of pause. The nano-hardness measured values referred to the as produced wrought, EBM and DMLS samples are 3.54 ± 0.14 GPa, 4.29 ± 0.27 GPa and 4.46 ± 0.31 GPa, respectively. There is no appreciable difference in nano-hardness values of AM parts, while the wrought material is clearly softer. It is worth noting that the mechanical properties, including hardness, are strictly related to the microstructure features (equiaxed, lamellar), their dimensions (coarse or fine) and texture (Tan et al. 2015; Kar et al. 2006). Thus, the slightly higher value of hardness on DMLS sample was not expected. However, although the DMLS microstructure is coarser than the EBM one (Figure 1), the thermal

history of DMLS process induced a martensite to alpha transformation that contributes to raise the overall hardness of the material (Facchini et al., 2010).

After the preliminary characterization of the as produced material, dry machining tests were performed on a CNC lathe. The aim of the turning operation is to clean and smooth the porous surface coming from the AM processes and to reduce the surface defects on the wrought material. The employed cutting tool is a CNMG 120404-23 H13A uncoated tungsten carbide, mounted on a PCLNR/L 2020k12 tool holder. Three conventional cutting speeds (V_c) for semi-finishing operations have been used: namely 50, 80 and 110 m/min, which are those recommended for Ti alloys by the tool manufacturer. The feed-rate (f) and the depth of cut (a_p) were set equal to 0.2 mm/rev and 0.2 mm respectively. A fresh cutting tool was used at each turning test in order to avoid the wear effect. Statistical repeatability was ensured by three tests repetitions at each cutting condition. The temperatures on the cutting region were also acquired for further analyses as reported elsewhere (Bordin et al., 2015; Imbrogno et al. 2016) revealing that the thermal gradient was always lower than 450 °C. Consequently, no phase transformation was observed since the β–transus temperature was not reached. Afterwards, the surface integrity of the machined surfaces has been probed thought morphological (roughness, optical and atomic force microscopies), chemical (x-ray diffraction) and mechanical (nano-indentation) analyses.

3. Results and discussions

3.1. *Surface morphology and microstructure*

The surface morphology was analyzed by means of a confocal white light 3D surface profilometer able to measure the roughness of the machined parts according to the DIN EN ISO 4288:1988. As shown in Figure 3, the surface mean roughness (R_a) generally decreased when the cutting speed increased. Furthermore, surface quality of wrought machined samples was found to be superior to those obtained by AM. The higher values of R_a found on the AM specimens can be attributed to their

lower ductility than the wrought samples (as also confirmed by the nano-hardness measurements performed on the as produced materials). In addition, it is also important to underline that the used cutting parameters for the semi-finishing operations are those conventionally suggested for wrought *Ti6Al4V* alloy, but not for additively manufactured products. The latter evidence also highlights that, in order to improve the surface quality, new sets of cutting speed, feed-rate and tools need to be investigated and optimized when additively manufactured samples are subjected to semi-finishing operations.

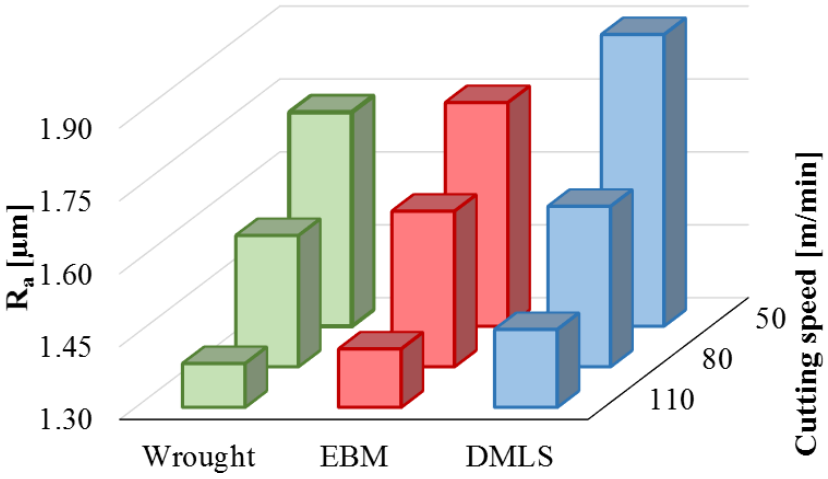

Figure 3. Surface mean roughness results (f = 0.2 mm/rev, a_p = 0.2 mm).

The microstructure analyses were carried out on an optical microscope and more detailed investigation into the affected layers was conducted by atomic force microscopy (AFM). The micrographs did reveal some metallurgical variation in terms of grain shape while the temperatures reached during the turning were lower than those needed to induce phase transformation. More in detail, it was observed that in all the three machined samples (EBM, DMLS and wrought) a thin layer of plastically deformed material was formed underneath the machined surface. In particular, the equiaxed grains (Figure 4 a) as well as the lamellar ones (Figure 4 b and c) were stretched and deformed along the cutting direction and both the grain size and the lamellae thickness were found to be smaller than those underneath the affected layer. This effect was more pronounced increasing the cutting speed. The highest variation was found at 110 m/min where the grain size of the machined

wrought samples were equal to 2.78 µm, while the lamellae thicknesses were 1.03 µm (DMLS) and 0.76 µm (EBM) as shown in Figure 5 (b). The AM processes play also a key role on the thickness of the affected layer as reported in Figure 5 (a). These results further confirm that the AM parts have different machinability behavior, even when they are produced from the same powder material.

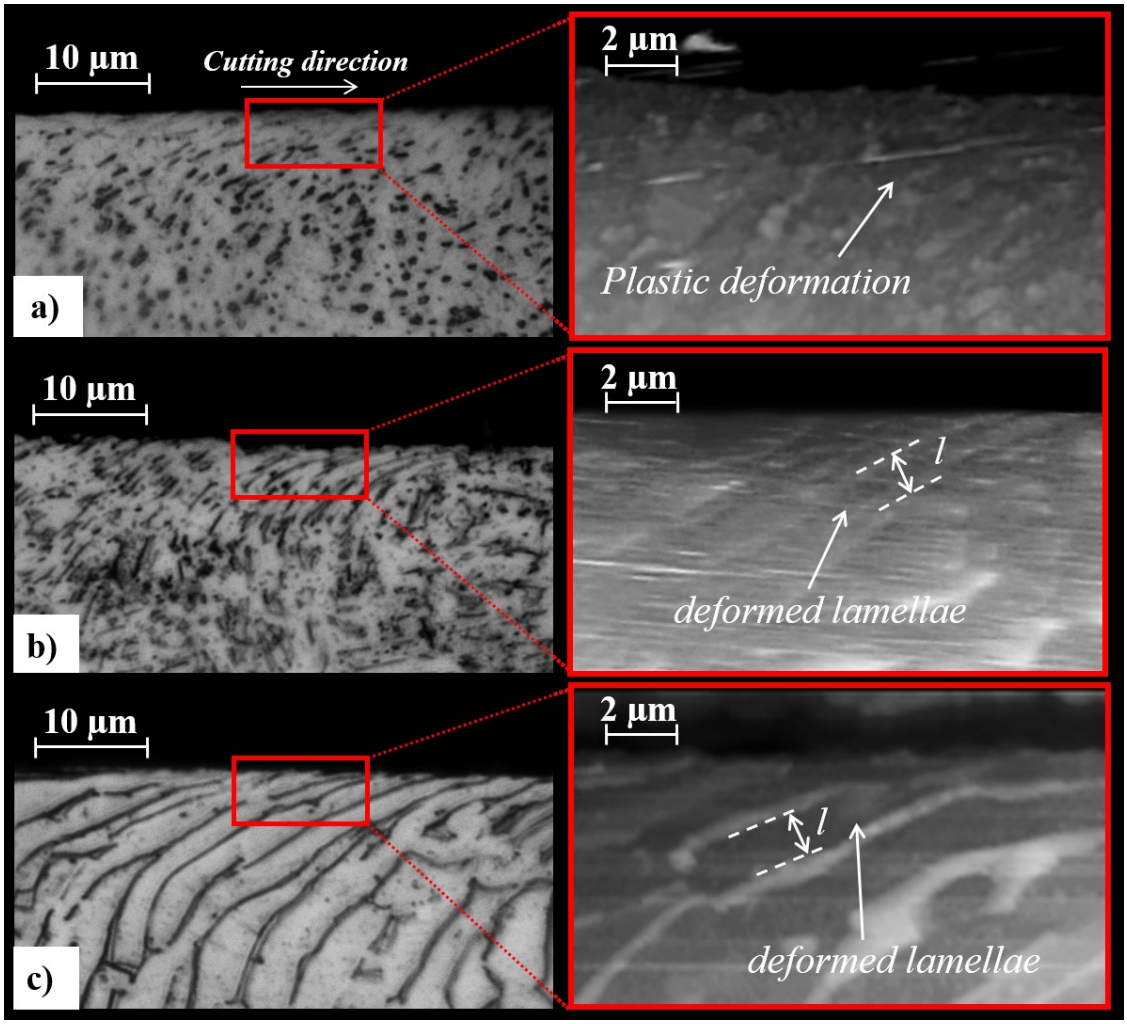

Figure 4. Optical micrographs and AFM microstructure analysis (V_c = 110 m/min, f = 0.2 mm/rev); (a) wrought; (b) EBM; (c) DMLS machined samples.

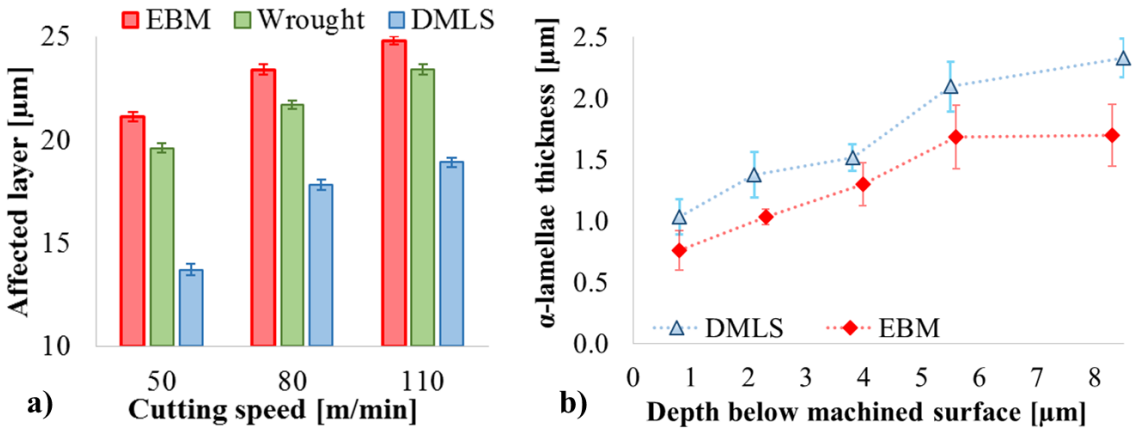

Figure 5. (a) Affected layer thickness; (b) α–lamellae thickness variation induced by turning on the AM samples (V_c = 110 m/min, f = 0.2 mm/rev).

3.2. Nano-hardness

The nano-hardness measurements were also carried out at the cross section of each machined sample from the surface through the depth direction and a set of ten measurements at the same distance from the surface was taken. The results were normalized with respect to the as received nano-hardness for each batch of material (EBM, DMSL and wrought) in order to easily compare the effects of turning operations (Figure 6 a and b). In fact, it is worth noting that as received wrought EBM and DMLS materials had different microstructure and hardness. In particular, the titanium alloy being produced by EBM and DMLS were measured to be 21% and 26% harder than the wrought material. The trends of the collected data highlight that the material beneath the machined surface, undergone to plastic deformation, was harder than the bulk. The highest hardness alteration was contained within 10 µm under the machined surface. The hardness measured within this region was averaged considering each material (wrought, EBM and DMLS) and its increment due to the machining operations (cutting speed of 50 m/min and 110 m/min) compared with the as received was considered. The wrought, EBM and DMLS showed a hardness increase of 9.40%, 15.70% and 6.25% respectively when machining at 50 m/min. The hardness raised even more when 110 m/min was selected as the cutting speed with a total increase of 22.5% for wrought, 29% for EBM and 10.20% for DMLS machined samples. Despite the

chemical composition of the material is unchanged (Ti6Al4V) for each batch of material, these results highlight that the three production techniques (wrought, EBM and DMLS) influenced the mechanical response to the machining processes. In fact, it is possible to observe that the EBM process permits to produce titanium parts that are significantly sensible to hardness changes induced by machining performed post-process operations if compared to other AM process such as DMLS.

The highest hardness values reached in the EBM machined samples are justified by the smallest α – lamellae thickness. Similar observations between mechanical properties (yield stress) and microstructure produced by EBM process were highlighted by Tan et al. (2015). These trends were also obtained in by Collins et al. (2009) and Al-Bermani et al. (2010). As overall, the decreasing grain size or lamellae thickness coupled with plastic deformations (strain-hardening) led to an increment of the surface hardness. Finally, the nano-hardness profiles also made possible to estimate the affected layer thickness, which was always ranging from 15 to 25 μm in depth slightly increased at increasing the cutting speed. These results also matched the experimental observations done by optical and AFM inspections.

Again, it is worth noting that the parameters suggested as "optimal" for cutting a wrought material can significantly affect the surface quality when AM products are machined.

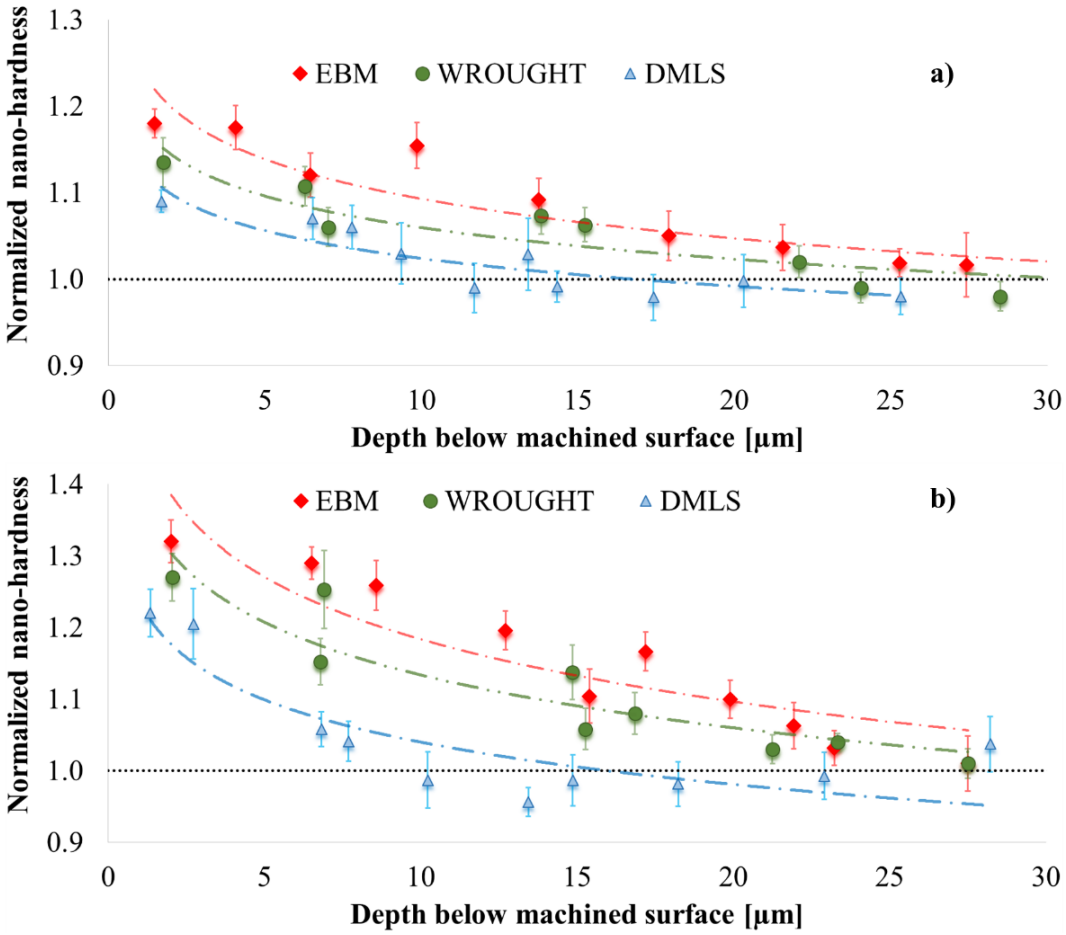

Figure 6. Normalized nano-hardness results for EBM, DMLS and wrought samples machined at (a) 50 m/min and (b) 110 m/min of cutting speed.

3.3. X-ray diffraction analysis

XRD analysis of machined surfaces were conducted to qualitatively understand the changes in texture at increasing cutting speed (Figure 7), using as produced materials as reference and carrying out comparison with the AFM analysis. The XRD patterns of the machined surfaces showed a broadening of the peaks and all the planes related to β–phase resulted weaker than the as produced as a consequence of cutting. These results were in agreement with those found by Velásquez et al. (2007) and Li et al. (2008). They stated that the changes in the XRD patterns, such as peaks broadening, are mainly due to the plastic deformation and the formation of dislocations produced by cutting processes

that determine micro strain and crystal lattice distortions, while changes of the intensity ratios can be attributed to the original texture changes.

Furthermore, no phase transformations or precipitate formations were identified by the XRD analysis, thus, confirming that the *β*–transus was never reached, as also verified by the measured temperatures during turning processes. The crystallographic orientation of the *α*–phase, that is characterized by a limited number of active slip systems, determines the ease of which slip occurs during turning process. In the case of the wrought *Ti6Al4V* machined sample, cutting speed influenced both the peak broadening and intensity ratio. Moreover, as the cutting speed increased a greater decrease of the intensity of the $(10\bar{1}0)$ prism plane, and $(10\bar{1}1)$ pyramidal plane of HCP *Ti-α* was observed, while (0002) *Ti-α* peak intensity correspondingly increased (Figure 7 a). The presence of a deformed region at the surface of the wrought machined samples was also confirmed by the AFM analysis as shown in Figure 4 (a).

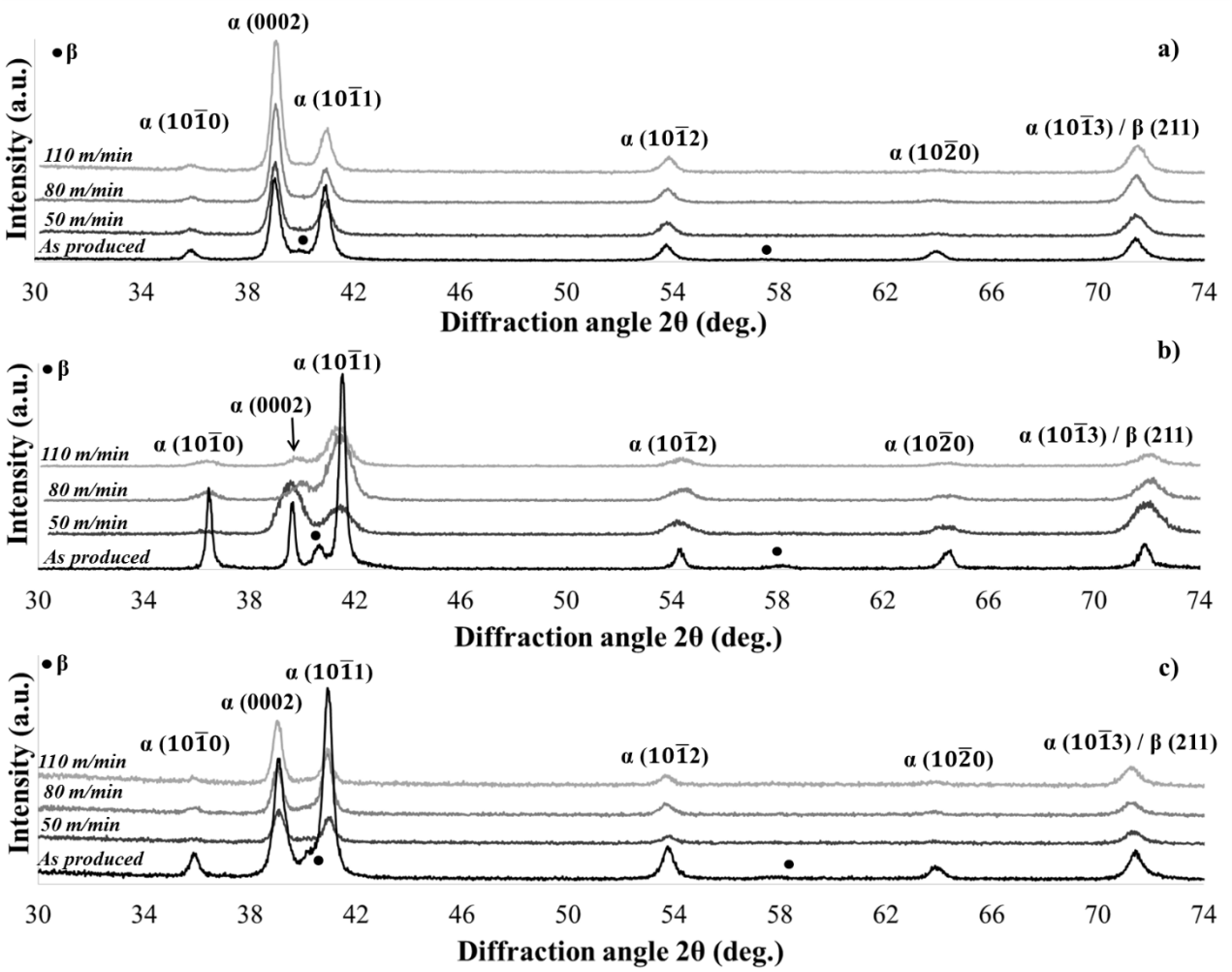

Figure 7. XRD patterns depending on the cutting speed; (a) wrought, (b) EBM and (c) DMLS machined samples.

The turning process deeply affected the texture of the EBM *Ti6Al4V* machined samples. In fact, as shown in Figure 7 (b), raising the cutting speed corresponded to increasing peaks broadening and decreasing peaks intensity. The variation of the intensity ratios in XRD patterns as well as high peak broadening indicate that grain refinement exists in the plastically deformed layer. This latter evidence is also confirmed by AFM analysis and measured *α*–lamellae thickness (Figure 5 b). The (10$\bar{1}$0), (0002) and (10$\bar{1}$1) *Ti-α* peask are the broader, suggesting that the *α* phase texture beneath the machined surface is significantly distorted, justifying also the higher hardness value measured on the EBM samples (Figure 6 a and 6 b) and its tendency to be more sensitive to machining processes.

Finally, with regards to the DMLS *Ti6Al4V* machined samples, it can be noticed that peak broadening in the obtained XRD patterns affects mainly $(10\bar{1}0)$ *Ti-α* plane (Figure 7 c). Furthermore, as the cutting speed increased the intensity shifted from $(10\bar{1}1)$ *Ti-α* peak to (0002) *Ti –α* peak, thus resulting in a change of texture. Overall XRD results confirm the occurrence of a microstructure deformation on the machined surface that also follows the cutting direction (Figure 4 c) as evidenced by AFM micrograph. Furthermore the more pronounced peak broadening observed in XRD patterns on EBM machined samples confirms the higher level of plastic deformation reached compared to wrought and DMLS.

Conclusions

Surface and subsurface modifications induced by turning operations on wrought and additively manufactured titanium alloys have been investigated. The morphological, chemical and mechanical analyses on the base and machined samples highlight the influence of the production process on the surface integrity of the finished parts. In fact, although the alloy composition is identical above all the samples, the microstructural characteristics and mechanical performances of the as produced parts and those machined are different. In fact, the trend of surface roughness highlights that the surface quality obtained on the wrought product is superior to those obtained on AM ones. Furthermore, AM materials show completely different behaviors in terms of affected layer size and surface and sub-surface hardness modifications. The overall results confirm that the machining process parameters are so far optimized for wrought materials highlighting the need to properly modify them for additively manufactured parts. According to the final application of the material, it is useful to know that a different hardness value can be achieved on the surface of machined AM parts, so that, for example, the product could be less prone to fretting fatigue initiation at surface than the wrought one. Also, the machining parameters can be further optimized taking into account the production technique. Although the overall trend of increasing hardness or reducing roughness at increasing

cutting speed is valid for all the different production techniques, it is crucial to quantify the differences within the amount of changes due to the same machining parameters. The presented work demonstrates that the machining process leads to different percentage of microstructural, topographical and mechanical alteration on the surface due to the initial production techniques (wrought, EBM and DMLS) even if the chemical composition of the materials remains unchanged. Thus, it is crucial for researchers and industry to properly select a process strategy compliant with the required surface quality when machining additively manufactured components.

References

Al-Bermani, S. S., Blackmore, M. R., Zhang, W., Todd, I., 2010, The Origin of Microstructural Diversity, Texture, and Mechanical Properties in Electron Beam Melted Ti-6Al-4V, Metall. Mater. Trans., 41A, 3422-3434.

ASTM International. Standard Terminology for Additive Manufacturing Technologies (F2792 - 12a). West Conshohocken, PA; 2012.

Bordin, A., Imbrogno, S., Rotella, G., Bruschi, S., Ghiotti, A., Umbrello, A., 2015, Finite Element Simulation of Semi-finishing Turning of Electron Beam Melted Ti6Al4V Under Dry and Cryogenic Cooling, Procedia CIRP, 31, 551-556.

Bordin, A., Sartori, S., Bruschi, S., Ghiotti, A., 2017, Experimental investigation on the feasibility of dry and cryogenic machining as sustainable strategies when turning Ti6Al4V produced by Additive Manufacturing, J. Clean. Prod., 142, 4142-4151.

Collins, P. C., Welk, B., Searles, T., Tiley, J., Russ, J. C., Fraser, H. L., 2009, Development of methods for the quantification of microstructural features in α+β-processed α/β titanium alloys, Mater. Sci. Eng. A, 508, 174-182.

Facchini, L., Magalini, E., Robotti, P., Molinari, A., 2009, Microstructure and mechanical properties of Ti6Al4V produced by electron beam melting of pre-alloyed powders, Rapid Prototyping J., 15/3, 171-178.

Facchini, L., Magalini, E., Robotti, P., Molinari, A., Höges, S., Wissenbach, K., 2010, Ductility of Ti6Al4V alloy produced by selective laser melting of prealloyed powders, Rapid Prototyping J., 16/6, 450-459.

Guo, P., Zou, B., Huang, C., Gao, H., 2017, Study on microstructure, mechanical properties and machinability of efficiently additive manufactured AISI 316L stainless steel by high-power direct laser deposition, J. Mater. Process. Tech. 240, 12-22.

Imbrogno, S. Bordin, A., Bruschi, S., Umbrello, D., 2016, Experimental analysis on semi-finishing machining of Ti6Al4V additively manufactured by direct melting laser sintering, AIP Conference Proceedings, 1769/1, Article number 080007.

Jawahir, I.S., Brinksmeier, E., M'Saoubi, R., Aspinwall, D.K., Outeiro, J.C., Meyer, D., Umbrello, D., Jayal, A.D., 2011, Surface Integrity in Material Removal Processes: Recent Advances, CIRP Annals – Manuf. Techn., 60/2:603-626.

Kar, S., Searles, T., Lee, E., Viswanathan, G. B., Tiley, J., Banerjee, R., Fraser, H. L., 2006, Modeling the Tensile Properties in β-Processed α/β Ti Alloys, Metall. Mater. Trans., 37A, 559-566.

Levy, G. N., Schindel, R., Kruth, J. P., Rapid Manufacturing and Rapid Tooling with Layer Manufacturing (LM) Technologies, State of the Art and Future Perspectives, 2003, CIRP Annals – Manuf. Techn., 52/2, 589–609.

Li, R., Riester, L., Watkins, T. R., Blau, P. J., Shih, A. J., 2008, Metallurgical analysis and nanoindentation characterization of Ti6Al4V workpiece and chips in high-throughput drilling, Mater. Sci. Eng. A, 472, 115-124.

Martina, F., Mehnen, J., Williams, S. W., Colegrove, P., Wang, F., 2012, Investigation of the benefits of plasma deposition for the additive layer manufacture of Ti–6Al–4V, J. Mater. Process. Tech., 212, 1377-1386.

Murr, L. E. 2015, Metallurgy of additive manufacturing: Examples from electron beam melting, Additive Manuf., 5, 40-53.

Puerta Velásquez, J.D., Bolle, B., Chevrier, P., Geandier, G., Tidu, A., 2007, Metallurgical study on chips obtained by high speed machining of a Ti6Al4V alloy, Mater. Sci. Eng. A, 452, 469-474.

Selcuk, C., 2011, Laser Metal Deposition for Powder Metallurgy Parts, Powder Metall., 54, 94–99.

Shamsaei, N., Yadollahi, A., Bian, L., Thompson, S.M., 2015, An Overview of Direct Laser Deposition for Additive Manufacturing; Part II: Mechanical Behavior, Process Parameter Optimization and Control, Additive Manuf., 8, 12–35.

Tan, X., Kok, Y., et al. 2015, Graded microstructure and mechanical properties of additive manufactured Ti–6Al–4V via electron beam melting, Acta Mater., 97, 1-16.

Thompson, S.M., Bian, L., Shamsaei, N., Yadollahi, A., 2015, An Overview of Direct Laser Deposition for Additive Manufacturing; Part I: Transport Phenomena, Modeling, and Diagnostics, Additive Manuf., 8, 36–62.

Yan, M., Yu, P., 2015, An Overview of Densification, Microstructure and Mechanical Property of Additively Manufactured Ti-6Al-4V – Comparison among Selective Laser Melting, Electron Beam Melting, Laser Metal Deposition and Selective Laser Sintering, and with Conventional Powder, Sintering Tech. Mater., 77-106.